The Viet Tran · Massimiliano Alvioli · Giha Lee · Hyun Uk An

Three-dimensional, time-dependent modeling of rainfall-induced landslides over a digital landscape: a case study

Abstract Physically based approaches for the regional assessment of slope stability using digital elevation model (DEM) topography usually consist of one-dimensional (1D) descriptions and often include more simplifying assumptions than realistic, three-dimensional (3D) analyses. We investigated a new application of the well-known, publicly available software TRIGRS (Transient Rainfall Infiltration and Grid-Based Regional Slope-Stability Model) in combination with Scoops3D to analyze 3D slope stability throughout a digital landscape in a time-dependent fashion, typically not implemented in three-dimensional models. TRIGRS simulated the dynamic hydraulic conditions within slopes induced by a rainstorm, and Scoops3D used the resulting pore water pressure for 3D stability assessment. We applied this approach to the July 2011 landslide event at Mount Umyeon, South Korea, and compared the results with the landslide initiation locations reported for this rainfall event. We described soil depth in the study area by three different simple models. Stability maps, obtained by the 1D (TRIGRS only) and 3D (TRIGRS and Scoops3D) time-dependent approaches, were compared with observations to assess the timing and locations of unstable sites via a synthetic index, previously developed specifically for dealing with point landslide locations. We highlight the performance of the 3D approach versus the 1D method represented by TRIGRS alone, as well as the consistency of the time dependence of the results obtained using the combined approach with the observations.

Keywords TRIGRS · Scoops3D · Landslide · Slope stability · Soil depth · Rainfall-induced · Infiltration · Pore water pressure

Introduction

Three-dimensional (3D) slope stability assessment on a regional scale has not been widely implemented because of its complexity, computational requirement, and the scarcity of required data. Most approaches assess slope stability using a one-dimensional (1D) infinite slope model on a raster cell-by-cell basis (Montgomery and Dietrich 1994; Pack et al. 1998; Baum et al. 2008; Valentino et al. 2014; An et al. 2016) or a two-dimensional (2D) slope stability model based on a series of cross-sections cut through the digital elevation model (DEM) (Miller and Sias 1998; Gu et al. 2014). Many researchers have stated that 1D and 2D analyses are acceptable in slope engineering not only because they are simpler, but also because they provide more conservative results than 3D models. As a matter of fact, 1D and 2D slope stability analyses typically provide results that suggest lower stability than that of 3D methods (Hungr 1987; Lam and Fredlund 1993; Okimura 1994; Arellano and Stark 2000; Huang and Tsai 2000; Xie et al. 2006b; Kalatehjari and Ali 2013; Chakraborty and Goswami 2016). These approaches, among other aspects of 1D or 2D assessments, may fail to model the actual mechanism of landslides (Bromhead et al. 2002). Indeed, natural slopes are not infinitely wide and, sometimes, it is difficult to accurately represent complex topography, even with 2D methods (Reid et al. 2000).

The simplifications implemented in 1D and 2D models typically correspond to a worst-case situation (Kalatehjari and Ali 2013) and thus have limitations. For example, it is difficult to estimate potential failure volumes, a factor of major relevance in debris flow modeling. Moreover, 1D or 2D analyses do not consider the direction of the slip surface. The sliding body is forced to move in an assumed direction (downslope), neglecting lateral, out-of-plane variations not only of the slope geometry, but also of geology, loading, water pressure, shear strength, and shape of the slip surface (Bromhead et al. 2002). Eventually, it is often assumed that the slip surface extends indefinitely, and 3D structure or end effects are considered negligible (Gens et al. 1988; Yu et al. 1998; Askarinejad et al. 2012). Therefore, the use of a 1D or 2D method may oversimplify the actual 3D mechanism and may result in non-conservative values of soil strength parameters obtained from the back analysis (Huang and Tsai 2000).

In this study, we applied the Transient Rainfall Infiltration and Grid-Based Regional Slope-Stability model (TRIGRS) (Baum et al. 2008), v2.1 (Alvioli and Baum 2016), and Scoops3D (Reid et al. 2015) for the 3D prediction of potential landslides caused by dynamic pore pressure changes resulting from the July 2011 rainstorm event at Mout Umyeon, Seoul, South Korea. The adopted method is a combination of a 1D, time-dependent infiltration model implemented in TRIGRS and a 3D slope stability assessment implemented in Scoops3D. The time-dependent 3D distributions of pressure head resulting from the 2011 rainstorm event were simulated using TRIGRS. The latest implementation of TRIGRS, version 2.1 (Alvioli and Baum 2016), is able to save an output containing 3D information on pressure head and soil saturation, readily usable in Scoops3D, which was then applied for a 3D assessment of landslides in the study area. To our knowledge, this is the first time that TRIGRS and Scoops3D are used in combination to obtain an overall time-dependent 3D slope stability assessment.

Park et al. (2013) analyzed the same rainfall event considered in this work. Their purpose was twofold: (1) simulation with TRIGRS to assess model performance in predicting failure locations via a custom performance index %LR$_{class}$ (explained in Eq. (7), "A performance index for point-like landslide data" section) and (2) use of a water runoff model bundled with TRIGRS to quickly select the path of the fluid masses mobilized by the triggering landslides. In particular, Park et al. (2013) concluded that the proposed %LR$_{class}$ index is a valuable tool for assessing the performance of pixel-based landslide predictions against empirical point landslide locations. In this study, we make use of a modified performance index, %LR$_{class}$, and extend the TRIGRS-based slope stability assessment with additional 3D modeling using Scoops3D. The description of the subsequent movement of the whole mass characterizing debris flow is governed by well-defined dynamics (Hürlimann et al. 2008;

Iverson 1997) and requires additional data, assumptions (Hungr 1995), and tools (Chianga et al. 2012; Gomes et al. 2013); these are beyond the scope of this work.

An important step in the procedure adopted here is the selection of input data and initial conditions: DEM, geotechnical and hydraulic parameters, initial soil water content, and cell-by-cell soil depth. In particular, we analyzed three simple existing soil depth models to compare the resulting accuracy in landslide prediction before selecting the most suitable one. To assess model performance, we used the observed landslide map that includes the initiation point locations of 25 sliding sites (Park et al. 2013; Baek and Kim 2015). Next, we compared the factor-of-safety (F_s) maps predicted by both the 1D and 3D approaches (hereafter referred to as F_{s1D} and F_{s3D}, respectively), in order to assess the accuracy in predicting the timing and location of failures.

This manuscript is organized as follows: the "Study area and available data" section describes the study area and the corresponding data required to run TRIGRS and Scoops3D. The "Methods" section describes relevant features of TRIGRS and Scoops3D, including a determination of the soil depth map, important input data for a physically based simulation, and the method adopted for dealing with point-like landslide data. Results are reported in the "Results and discussion" section, where we discuss the performance of the combination of TRIGRS and Scoops3D in predicting landslide occurrence timing and location, comparing the predicted stability maps achieved by the 1D approach (using TRIGRS) and the 3D approach (using Scoops3D). Conclusions are presented in the "Conclusions" section.

Study area and available data

Mount Umyeon is located in the southern part of Seoul (Fig. 1a). The coordinates are 37° 27′ 00″–37° 28′ 55″ N latitude and 126° 59′ 02″–127° 01′ 41″ E longitude. The area is characterized by steep hills, gullies, and valleys with an average slope of 15° (slopes usually less than 40°). Elevations range from 50.0 to 312.6 m. The mountain is primarily composed of highly weathered banded gneiss with subordinate granitic gneiss. Also, with the existence of multiple faults combined with geomorphological defects caused by military activities, Mount Umyeon is highly susceptible to slope instability and sliding (Baek and Kim 2015).

The study site (Jeonwon-maul) (Fig. 1b) is located in the west part of Mount Umyeon. In this area, 25 slope failure locations were reported on the morning of July 27, 2011. Although the precise timing of the landslide observation data is not available, it was reported by local people that these mass movements occurred between 07:00 and 09:00 KST (Korean Standard Time). The locations of the head scarps of all the landslides (Fig. 1b) were recorded using portable GPS and verified with field survey. Figure 2 presents a closer look of the landslide initiation zone in the study area. In the gneiss, most foliations are seen coming from the southeast direction, opposite the slope gradient.

Digital elevation model and slope map

The DEM resolution for landslide modeling should be chosen depending on the quality and resolution of the input data, the size of the study area, the resolution required for the output maps, and the relative size of the landslide scars. For most 1D grid-based approaches, a rigorous relationship between cell size and the
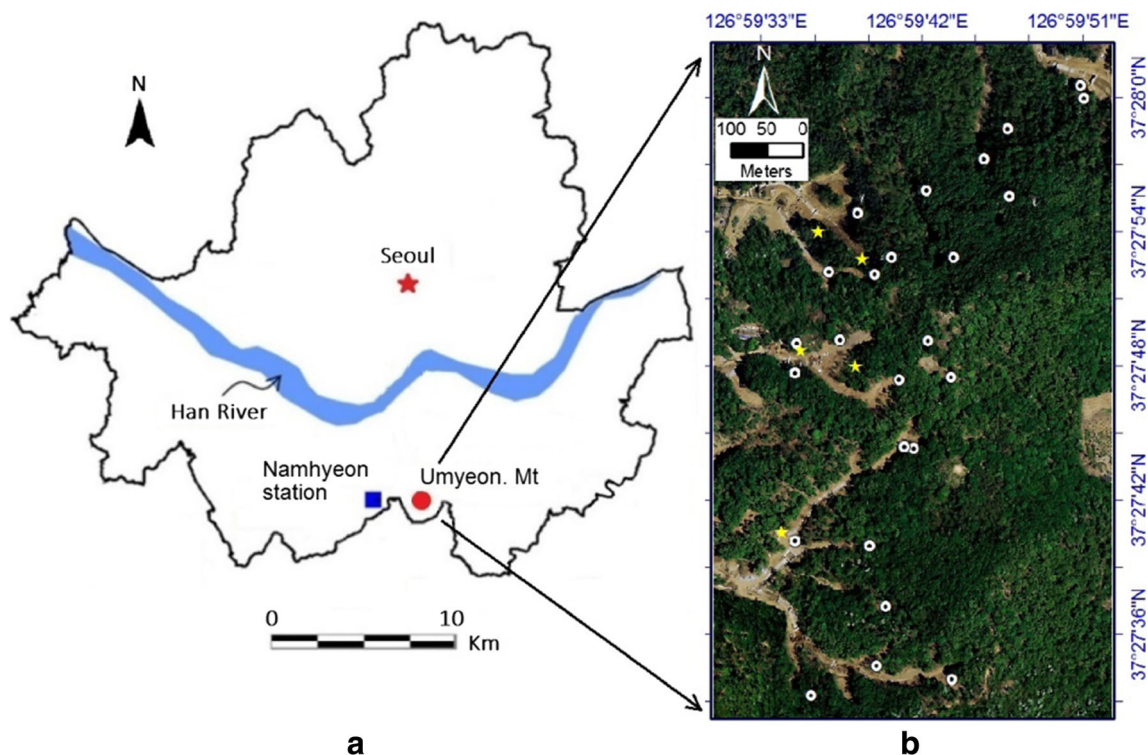

Fig. 1 Location of the study area. **a** Location of Umyeon Mountain. **b** The study site. Each dot represents a slide site, and the stars show the sampling locations

Fig. 2 A typical landslide initiation zone at the study site (data from Baek and Kim, 2015)

Fig. 3 Digital elevation model. The circles show the observed slide sites

performance of landslide prediction models is yet to be established (Viet et al. 2016). In the case of Scoops3D, the DEM resolution must have sufficient resolution to characterize the topographic conditions that influence stability. Increasing the resolution of the DEM provides more active columns for a given trial surface and thereby increases the accuracy of the calculated landslide volume and area (Reid et al. 2015), provided that the additional available data is of comparable resolution and adequate accuracy. According to Reid et al. (2010), a trial failure should encompass at least 200 columns to produce both the 3D F_s map and potential failure volume results within 1% of failures represented by thousands of columns.

The 1-m spatial resolution DEM (Fig. 3) data was computed from light detection and ranging (LiDAR) data collection (Tran et al. 2017). Other input maps such as the slope map and the flow direction map required for TRIGRS and Scoops3D were created from the DEM using ArcMap.

Soil parameters

According to Kim et al. (2014), the topsoil is classified as SM (sand and silt) in the Unified Soil Classification System. However, the weathering production of gneiss, which is dominant in the study area, is enriched with fine particles and clay minerals. Therefore, a thin clayey layer was observed at the transition layer between the colluvium and the gneiss bedrock (Baek and Kim 2015). Regarding the input data required for TRIGRS and Scoops3D, field investigations, field tests, and laboratory tests were conducted to define the unit weight, shear strength, saturated hydraulic conductivity, and soil water retention parameters. Figure 1b shows the sampling locations, and Fig. 4 shows the results of tests performed to define the soil water retention curve, which was used to characterize the unsaturated behavior of the soil. The soil shear strength, which plays an important role in slope stability, was measured using consolidated undrained tests. To reduce uncertainty, three tests on samples from three different locations were conducted, and the most critical value was conservatively selected. Table 1 lists all the soil geotechnical values used in the simulations.

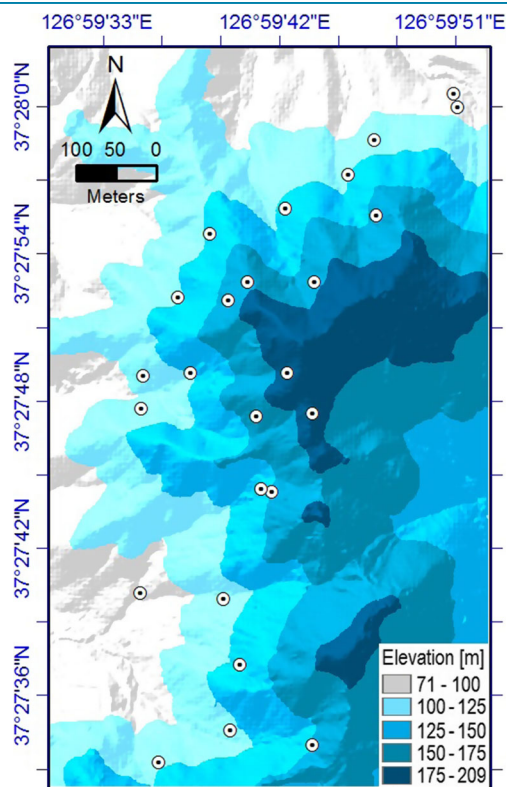Supplementary parameters, including the diffusivity D_o and the initial surface flux I_z, cannot be defined by testing. These parameters were determined using empirical equations from the literature. In the study area, as suggested by Park et al. (2013) and Viet et al. (2016), D_o was assumed to be 100 times the value of K_s based on the soil type, and I_z was assumed to be 0.01 of the K_s because of the hot, dry conditions during the month of July.

The issue of soil variability (Raia et al. 2014; Mergili et al. 2014) is not addressed in this study because it is beyond the scope of this work.

Rainfall information

Mount Umyeon is located in the temperate monsoon zone. The area is usually hot and humid, with abundant rainfall in summer and with cold and dry conditions in winter. The average annual precipitation ranges from 1100 to 1500 mm, with 70% of the annual average recorded between June and September. The event of July 27, 2011, is the most catastrophic of all recorded debris flows, due to its high intensity and long rainfall duration. This particular event was reported not only in the Umyeonsan region but also across most of Korea (Jeong et al. 2015).

According to Baek and Kim (2015), the main factor causing landslides in the study area is precipitation, which can be divided into two different domains based on temporal variations: antecedent rainfall and daily rainfall. Indeed, based on rainfall records, Baek and Kim (2015) showed that landslides might be triggered by high-intensity daily rainfalls following long-term antecedent precipitation. Before the landslide events, the antecedent rainfall reached 463.0 mm within 2 weeks, and then, heavy daily rainfall reached 342.5 mm. In this study, we used the rainfall data that
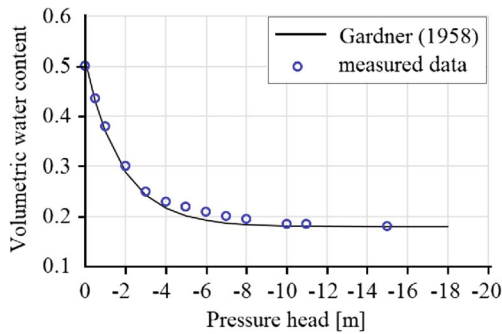
Fig. 4 Graph showing the soil water characteristic curve of soils in the study area

triggered the landslides in Mount Umyeon as recorded at the Namhyeon station between July 26 and 27, 2011. The analyzed duration is a period of 24 h, from 16:00 KST on July 26 to 16:00 KST on July 27 (Fig. 5).

Methods

The methodology adopted in this work is a chain of two models. We first executed the 1D model TRIGRS to calculate pore water pressure (PWP) values in a spatially distributed and time-dependent manner. Then, we conducted Scoops3D for the subsequent 3D slope stability assessment, using PWP information provided previously. The 1D and 3D definitions of the factor of safety, F_{S1D} and F_{S3D}, respectively, are described below. Crucial for TRIGRS execution, in addition to DEM and soil parameters discussed in the "Study area and available data" section, is the determination of the initial groundwater table and spatially distributed soil depth. Crucial requirements of the Scoops3D program are the spatial constraints on potential sliding surfaces, namely, the search grid for random trials. The methodology adopted here to determine such quantities is described in this section. Eventually, we discussed an adaptation of an existing synthetic index that we used to assess the performance of model predictions, both 1D and 3D, against point landslide data.

The transient rainfall infiltration and grid-based regional slope stability model

The TRIGRS model was developed to model the timing and distribution of rainfall-induced shallow landslides (Baum et al. 2008). In the model, the time variable is represented by time-dependent

rainfall infiltration, resulting from storms that can have durations ranging from hours to days, potentially resulting in simulations of considerable time and computing requirements (Alvioli and Baum 2016). TRIGRS combines an analytical solution to assess the response of PWP to rainfall infiltration into the unsaturated soil, with an infinite slope stability simulation to predict the spatial and temporal occurrences of landslides (Baum et al. 2010). PWP and F_{S1D} are correspondingly simulated on a cell-by-cell basis and can be displayed in a geographical information system (GIS) (Baum et al. 2008). Different outputs of the model can be saved at multiple times during the simulation, and an additional output file containing PWP information directly readable by Scoops3D can be exported.

In TRIGRS, four options for infiltration modeling are available: (1) saturated soil with infinite basal boundary depth, (2) saturated soil with finite basal boundary depth, (3) unsaturated soil with infinite basal boundary depth, and (4) unsaturated soil with finite basal boundary depth. In this study, based on the characteristics related to the geological and initial conditions of the study site discussed previously, the unsaturated, finite-depth model was selected. The boundary conditions assumed in the selected infiltration model for our study area are sketched in Fig. 6.

Rainfall infiltration and vertical flow fluxes through the unsaturated zone are described in TRIGRS by the Richards equation. The equation is implemented in the linearized form of Gardner (1958), which makes use of an exponential ansatz for the saturated hydraulic conductivity and the moisture content.

Slope stability is assessed in TRIGRS within the infinite-slope approximation assuming failure planes parallel to the ground surface (Taylor 1948). Forces acting between neighboring grid cells in the sliding mass are neglected. The stability condition of the slope is characterized by a factor of safety, F_{S1D}, which is the ratio of the resisting basal Coulomb friction to the gravitationally induced downslope basal driving stress. The ratio is calculated at an arbitrary depth Z for each grid cell as follows:

$$F_{S1D}(Z, t) = \frac{\tan\phi'}{\tan\delta} + \frac{c' - \psi(Z, t)\gamma_w \tan\phi'}{\gamma_s Z \sin\delta \cos\delta}, \qquad (1)$$

where c' is the effective soil cohesion, ϕ' is the soil effective friction angle, ψ is the pressure head as a function of depth Z and time t, δ is the slope angle, and γ_w and γ_s are the unit weights of water and soil, respectively. As usual, failure is predicted when $F_{S1D} < 1$, and stability holds when $F_{S1D} \geq 1$. Additional details about the

Table 1 Geotechnical and hydraulic parameters of the soil used for the simulations in the study area

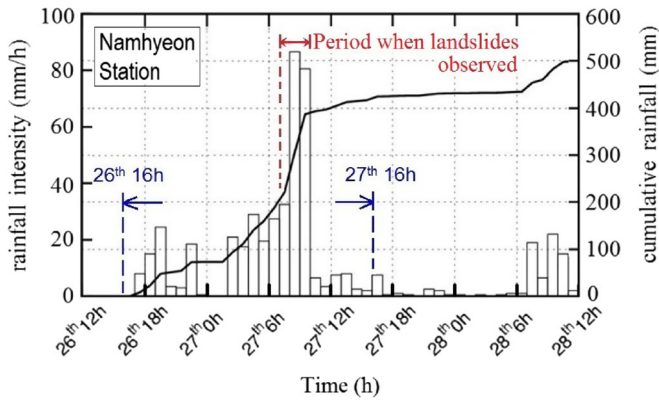| Parameters	Symbol	Unit	Value range	Selected value
Hydraulic conductivity	K_s	ms^{-1}	8.0×10^{-6}	8.0×10^{-6}
Unit weight of soil	γ_s	kN m^{-3}	17.5–18.5	18
Soil cohesion	c'	kN m^{-2}	9.6–11.5	9.6
Apparent root cohesion	C	kN m^{-2}	0	0
Soil friction angle	ϕ'	Degrees	25.5–26.4	25.5
Saturated volumetric water content	θ_s	–	0.5	0.5
Residual volumetric water content	θ_r	–	0.18	0.18

Fig. 5 Rainfall intensity and cumulative rainfall from 12:00 KST July 26 to 12:00 KST July 28, 2011, as recorded at the Namhyeon station. The study period is from July 26, 16:00 KST, to July 27, 16:00 KST

assumptions and operation mode of TRIGRS can be found in Baum et al. (2008) and Alvioli and Baum (2016).

The TRIGRS model was used in conjunction with GIS software. GIS is a powerful tool for spatially distributed data processing, a technology that has recently shown vast improvement and that is widely used in landslide assessment (Trigila et al. 2010; Jia et al. 2014; Quiu et al. 2007). TRIGRS works on a cell-by-cell basis, and GIS software is a natural choice for preparing the necessary input gridded data in ASCII format. This feature is particularly useful when an analysis requires repeated runs with different input data, as is the case here for the selection of different soil thickness models, described below.

GIS software is a valuable working tool to prepare input data for exploring different combinations of input geotechnical
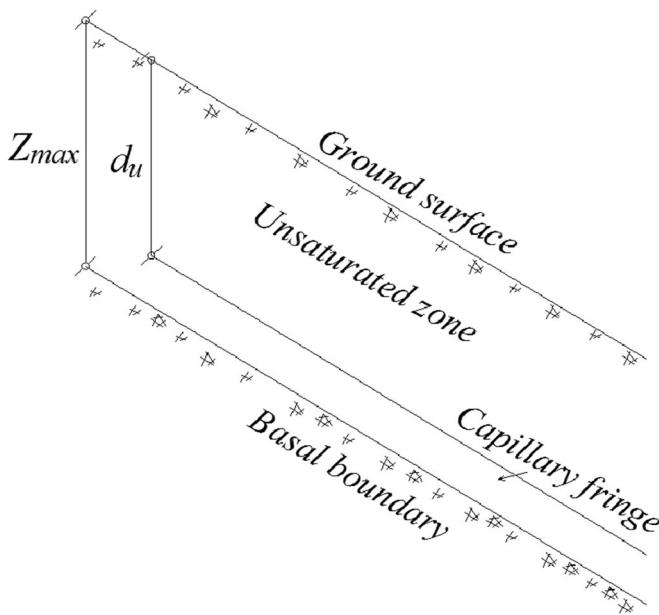

Fig. 6 Boundary conditions assumed in TRIGRS for Mt. Umyeon. The initial groundwater table coincides with the bedrock layer; d_u is the thickness of the unsaturated layer, and Z_{max} is the depth of the basal boundary, modeled in three different ways in this study

parameters, which can be provided in TRIGRS either as uniform values across the study area or as grids with different zones in which parameters assume different values. The latter case is typically the result of the intersection of geological, lithological, and land use layers in a GIS environment. Exploration of various random combinations of input parameters is also used to account for the variability of parameters in the real world, thoroughly investigated by Raia et al. (2014). This approach was not pursued in this work, as our aim is to assess the validity of time-dependent 3D slope stability modeling. We maintain that the probabilistic approach could be included, and the variability of soil characteristics would be reflected somewhat in the 3D modeling results.

3D slope stability with the Scoops3D model

The Scoops3D program (Reid et al. 2015) uses the 3D "method of columns" to determine the stability of potential slip surfaces, assumed to be the intersections of spherical trial surfaces with the soil columns defined by the DEM grid cells. For each potential failure, Scoops3D calculates the stability against the rotation along the portion of the spherical surface, using the 3D version of either Bishop's simplified method or the ordinary limit equilibrium method (LEM) (Reid et al. 2015).

An analysis of the literature shows that most 3D slope stability LEMs are derived from 2D LEMs with similar assumptions (Chakraborty and Goswami 2016). There are three popular approaches for column-based 3D slope stability analyses: (1) the ordinary column-based model of Hovland (1977), (2) the 3D extension of Bishop's simplified method (Hungr 1987), and (3) the 3D extension of Janbu's simplified method (Hungr et al. 1989). Among these three methods, the extension of Bishop's method typically provides reliable F_{s3D} results that are close to more recent and rigorous LEMs (Spencer 1967; Hungr 1987; Lam and Fredlund 1993; Reid et al. 2015).

The Scoops3D model was originally developed to assess the stability of volcano edifices and has been successfully tested at several locations including the Casita and San Cristobal Volcanoes of Nicaragua (Vallance et al. 1998); Augustine Volcano, Alaska (Reid et al. 2010); southwestern Washington (Brien and Reid 2007); and Mount St. Helens, Washington (Reid et al. 2010). As compared to many 3D models, the advantage of Scoops3D is that it considers the topography described by the DEM to locate various potential sliding masses throughout the landscape, not only for an individual landslide on a predefined hillslope.

Scoops3D examines the overall force balance of a rigid mass potentially sliding along a predefined failure surface (Reid et al. 2015). The equilibrium of forces and moments are ensured for each column as well as for the total slip surface mass. In general, all LEMs define F_{s3D} as the ratio of the average shear resistance (strength), s, to the shear stress, τ, needed to maintain the limiting equilibrium along a predetermined trial surface:

$$F_{s3D} = \frac{s}{\tau}. \tag{2}$$

As usual, in Eq. (2), $F_{s3D} \geq 1$ results in limiting equilibrium, and $F_{s3D} < 1$ suggests that the slope is theoretically unstable. For the present analysis, we selected the 3D extension of Bishop's simplified method of slices for LEMs (Bishop 1955) because it offers a simple and efficient approach which is applicable to a wide range

of practical problems (Hungr et al. 1989; Yu et al. 1998). This method assumes that the side forces on soil columns are horizontal (with no net shear stress between slices), and can, therefore, be dismissed. In Scoops3D, the same assumptions are made for columns, following the method presented by Hungr (1987). The average shear resistance τ, acting on a potential failure surface, is defined by the Coulomb-Terzaghi failure law (Brien and Reid 2007):

$$\tau = c' + (\sigma_n - u)\tan\phi', \qquad (3)$$

where c' is the soil cohesion, ϕ' is the angle of internal friction, σ_n is the total normal stress acting on the failure surface, and u is the PWP acting on the shear surface.

In unsaturated soil media, PWP is negative, thus increasing shear resistance (Eq. (3)). Scoops3D has an option to allow the incorporation of partially saturated PWP. However, in this study, since the data used for simulation is limited, the impact of negative PWP was ignored, and all negative values were replaced with zeroes (Reid et al. 2015). Summing for all columns within the potential slip surface, the factor of safety F_{S3D} for the 3D analysis can be calculated as follows:

$$F_{s3D} = \frac{\sum R_{i,j}\left[c_{i,j}A_{h_{i,j}} + \left(W_{i,j} - u_{i,j}A_{h_{i,j}}\right)\tan\phi_{i,j}\right]/m_{\alpha_{i,j}}}{\sum W_{i,j}\left(R_{i,j}\sin\alpha_{i,j} + k_{eq}e_{i,j}\right)}, \qquad (4)$$

where $A_{h_{i,j}}$ is the horizontal area of the trial surface at the base of the column (i, j), $R_{i,j}$ is the resisting force arm or the failure surface radius, $W_{i,j}$ is the weight of the column (i, j) above the slip surface, $u_{i,j}$ is the PWP acting on the shear surface, $\alpha_{i,j}$ is the apparent dip of the column base in the direction of rotation, k_{eq} is the horizontal pseudo-acceleration coefficient from earthquake shaking, $e_{i,j}$ is the horizontal driving force moment arm for a column (equal to the vertical distance from the center of the column to the elevation of the axis of rotation), and $m_{\alpha_{i,j}} = \cos\varepsilon_{i,j} + \left(\sin\alpha_{i,j}\tan\phi_{i,j}\right)/F_{s3D}$, with $\varepsilon_{i,j}$ as the true dip of the trial surface. Note that in 3D, the value of all the parameters with subscripts (i, j) may vary from column to column. Additional details explaining Eq. (4) are described in Reid et al. (2015).

Spatial distribution of soil depth

Spatial patterns in soil depth arise from the complex interactions of many factors such as topography, parent material, climate, and biological, chemical, and physical processes (Tesfa et al. 2009). Also, the thickness of the soil can vary as a function of many different and interplaying factors, such as the underlying lithology, the slope gradient, the hillslope curvature, the upslope contributing area, and the vegetation cover. As a result of the high variability in these parameters, soil thickness distribution is challenging to model. Due to the substantial increase in the use of soil depth in hydrological models, numerous approaches for estimating the spatial patterns of soil thickness have been proposed. Salciarini et al. (2006) proposed an exponential soil thickness model linking soil thickness to slope angle. Tesfa et al. (2009) developed statistical models to predict the spatial patterns of soil depth

over complex terrains from topographic and land cover attributes. Pelletier and Rasmussen (2009) used high-resolution topographic data to model soil thickness assuming a long-term balance between soil production and erosion. Catani et al. (2010) proposed an alternative methodology linking soil thickness to the gradient, horizontal and vertical slope curvatures, and relative position within a hillslope profile. In all cases, however, detailed data on soil properties and thickness can be difficult to obtain for a large area. Thus, it remains frequently challenging to acquire the complete set of input data necessary to use analytical GIS-based landslide models (Salciarini et al. 2006). Another possible approach is the random determination of soil thickness, provided that suitable probability distribution functions can be modeled (Raia et al. 2014). The dependence of TRIGRS results on soil thickness was also investigated by Alvioli et al. (2016). In this study, soil thickness was assigned by comparing the landslide results predicted by three common simple models as described below:

1. U model: Soil depth is assumed to be uniformly distributed with a thickness of 2.0 m, as suggested by Park et al. (2013).
2. S1 model: Soil depth is assumed to be linearly distributed with the slope angle. In this approach, as suggested by Viet et al. (2016), the relationship imposes the maximum slope angle corresponding to the minimum soil depth (0.1 m), and the minimum slope angle is related to the maximum soil depth (3.5 m). These minimum and maximum soil depths of the colluvium followed the fieldwork report of the Korean Society of Civil Engineers (2011). Following this approach, the soil depth of an arbitrary pixel (y) can be interpolated using its slope angle (x) by the function $y = -0.0486x + 3.5$. The resulting soil depth map is presented in Fig. 7a.
3. S2 model (Saulniera et al. 1997): The effective soil depth is assumed to be expressed by

$$y_i = y_{max}\left[1 - \frac{\tan(x_i) - \tan(x_{min})}{\tan(x_{max}) - \tan(x_{min})}(1 - \alpha)\right], \qquad (5)$$

where $\alpha = y_{min}/y_{max}$, y_{min} and y_{max} are the minimum and maximum values of effective soil depth, and x_i is the slope angle at point i. Using Eq. (5), the soil depth of an arbitrary pixel (y_i) is interpolated using its slope angle (x_i) by the function $y_i = 3.5 - 1.2415\tan(x_i)$. The resulting soil depth map is presented in Fig. 7b.

Determination of initial conditions, pore water pressure, and slip surfaces

Before simulating the temporal dependency of hydraulic conditions induced by the rainstorm, the initial groundwater table was set. For the use of TRIGRS, initial conditions include the initial flow field throughout the study area and the initial groundwater table depth (Baum et al. 2008). The initial flow field can be characterized by DEM data, while field observations are often required to characterize the initial groundwater table depth. Since soil water observations related to the initial conditions of the
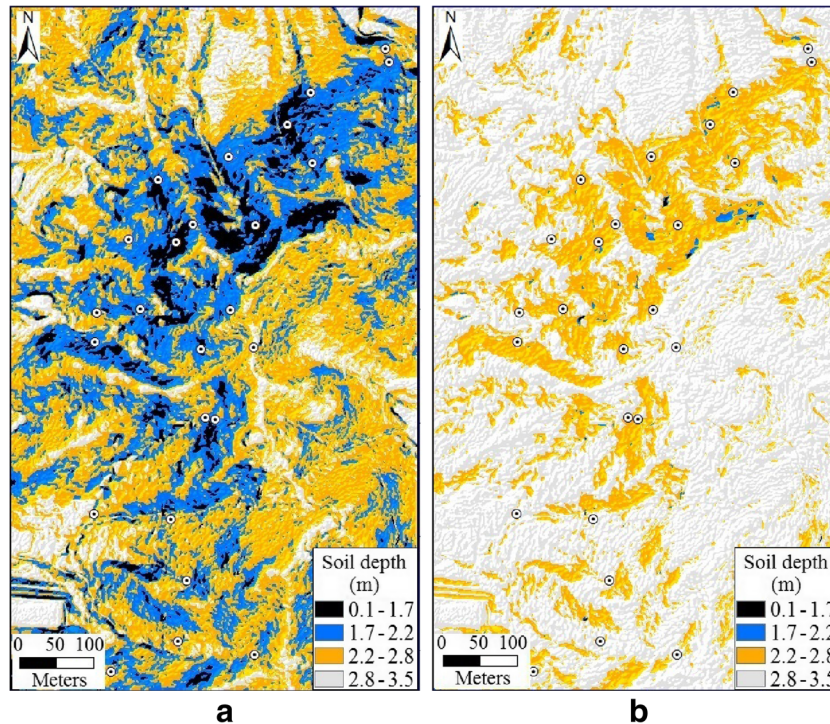
Fig. 7 Soil depth map. **a** S1 model and **b** S2 model, described in the "Spatial distribution of soil depth" section. The U model corresponds to uniform soil depth and is not depicted in the figure

groundwater level were not available for this study area, the groundwater table prior to the rainstorm was assumed to coincide with the bottom of the colluvium layer following the same assumption for this study area from Kim et al. (2010), Park et al. (2013), Viet et al. (2016), and Tran et al. (2017). In this scenario, rainfall caused the initial groundwater level to rise and changed the distribution of the pressure head.

The difficulty in determining the PWP field stems from the complex and spatial- and time-dependent groundwater flow. Scoops3D allows selecting from different methods to account for the PWP effects in the 3D slope stability evaluation. Each of these options includes different assumptions regarding the use of PWP for stability assessment that can cause small variations in the stability equation used in Scoops3D. In this study, we conducted an analysis using the 3D description of the pore pressure head, using TRIGRS to simulate the dynamic hydraulic conditions experienced during a rainstorm. Scoops3D, then, used the resulting PWP for the 3D stability assessment.

In 3D slope stability analysis, a search with many (ideally, infinite) trial surfaces is needed due to the variations in local topography, material properties, and PWP (Reid et al. 2015). Scoops3D thoroughly examines the DEM for potential sliding masses based on well-defined size criteria and a user-defined search grid (Fig. 8). The former is defined as the range of failure volume or the area of potential sliding masses specified, possibly based on field observations. The latter is determined by input parameters, including the vertical and horizontal extents of the search lattice (Fig. 8).

The average volume and the total area of all observed landslides in the study area are available from Baek and Kim (2015). However,

since soil depth data is lacking, in this work, the area criteria were used with some limitations. The total sliding areas in the Jeonwon-
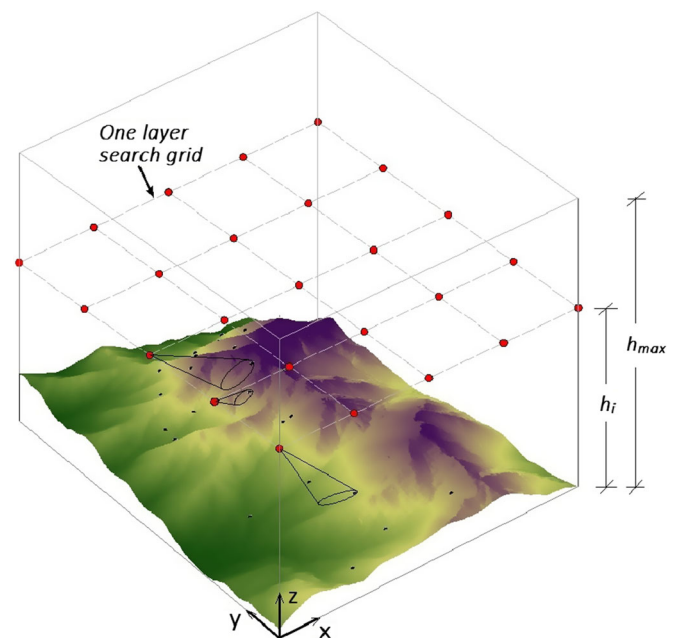

Fig. 8 3D overview of the study area DEM with several potential sample trial slip surfaces. A layer of the search grid is shown above the DEM. Each point on the grid denotes the center of multiple spherical trial surfaces with differing radii. H_{max} is the maximum elevation of the search grid, and h_i is the elevation of the ith search grid center

Table 2 LR$_{class}$ (Eq. (6)) evaluation of the TRIGRS model as a function of the U, S1, and S2 soil depth models described in the "Spatial distribution of soil depth" section. The corresponding soil depth maps are shown in Fig. 7, and the resulting F_{s1D} maps are shown in Fig. 9. The relationships between the various columns (a, b, c, d) are shown for clarity. Note that columns (a) and (c) both make use of empirical data, while column (d) does not

F_s class	Observed sites (a)			Observed sites (%) (c) = (a)/25 × 100			Predicted area (%) (d)		
	U	S1	S2	U	S1	S2	U	S1	S2
$F_s < 1$	13	15	6	52.0	60.0	24.0	21.36	20.10	7.24
$F_s \geq 1$	12	10	19	48.0	40.0	76.0	78.64	79.90	92.76
Sum	25	25	25	100	100	100	100	100	100

maul and Bodeok-sa regions, overlapping our study site, are 431.2 m² (with 22 sliding sites) and 274.2 m² (with 14 sliding sites), respectively (Baek and Kim 2015). Testing Scoops3D using multiple values of the maximum area criteria, we noted that the unstable areas were unchanged when this maximum value was larger than 305 m² (about 15 times the average size of landslides in the study area) and that the area of predicted unstable areas decreased with a reduction in this maximum size criteria. Therefore, although data related to the specific size of the observed landslides was unavailable, we managed to constrain potential landslide areas to a range of 20 m² (4 m × 5 m) to 305 m³ to evaluate the performance of the model in predicting the timing and location of the landslide initiation points.

Another relevant parameter here is the elevation range of the search grid used to specify the centers of the trial sliding surfaces located above the DEM (Fig. 8). The grid is defined by input parameters including the vertical and horizontal extents of the search lattice, the minimum of which was assumed to correlate with the elevation of the observed sliding sites. We increased the maximum elevation until no change was found on the predicted F_{s3D} map. Following this procedure, the vertical extent of the search lattice was set from 87 to 195 m in all Scoops3D runs. The horizontal extent of the search grid was the same as that of the DEM. The radius of the spherical trial surface at each search grid point was incremented by 1 m until the area of the corresponding potential landslides reached the maximum specified value (305 m² in our case) of the input area.

By default, the program performs a search for the least stable failure mass at many depths. During the search, the least stable potential failures are identified through an extensive comparison of all potential failures that fall within the specified size criteria (area/volume). The analysis results in maps representing the relative stability of each cell in the study area, along with the locations and volumes of the overall least stable potential landslides (Reid et al. 2015). Moreover, unlike 1D approaches, Scoops3D always computes F_{s3D} for the slip direction in the overall slide direction, defined as the average ground surface for each DEM cell encompassed by the potential failure mass (Reid et al. 2015).

A performance index for point-like landslide data

In this study, we needed to overcome the mismatch between the outcome of the physically based simulation (given on a cell-by-cell basis by construction) and the available landslide data (known only in point-like locations). This is a common situation, especially if the simulation concerns large areas, for which the collection of accurate landslide data is difficult or impossible. We performed a comparison with the observed landslide locations using the %LR$_{class}$ index (Park et al. 2013), developed specifically to deal with situations when the boundaries of observed landslides are not available, but where their locations are known. The F_s maps were classified into different classes: an intermediate quantity, LR$_{class}$, is defined as the ratio of the number of sliding sites contained in each F_s class to the total number of actual landslide sites (25 sites in our case), according to the predicted percentage of area in each class of F_s (Eq. (6)). The %LR$_{class}$ index for the F_s class i (%LR$^i_{class}$) is the corresponding percentage with respect to the total value of LR$_{class}$ of all the i classes of F_s (Eq. (7)).

The advantage of using the %LR$_{class}$ index is that it considers both the predicted stable and unstable areas and thus significantly decreases over-prediction. The %LR$_{class}$ index indicates that if a slope failure occurs, the predicted unstable area ($F_s < 1$) has a chance equal to the %LR$_{class}$ of including an actual slope failure. A larger value of %LR$_{class}$ corresponds to a lower over-prediction by the model (Park et al. 2013). We improved the definition of %LR$_{class}$ suggested by Park et al. (2013) as follows:

$$\text{LR}_{class} = \frac{\%of\ contained\ slope\ failure\ locations\ in\ each\ F_s\ class}{\%of\ predicted\ areas\ in\ each\ F_s\ class},$$

(6)

$$\%\text{LR}^i_{class} = \frac{\text{LR}^i_{class}}{\sum_{i=1}^{n}\text{LR}^i_{class}}.$$

(7)

In the original definition of LR$_{class}$ by Park et al. (2013), the denominator reads as "% of predicted slope failure areas in each

Table 3 LR$_{class}$ (Eq. (6)) and %LR$_{class}$ (Eq. (7)) evaluation of the TRIGRS model as a function of the U, S1, and S2 soil depth models. The relationships between the various columns (a, b, c, d) from Table 2 and columns (e) and (f) below are shown for clarity

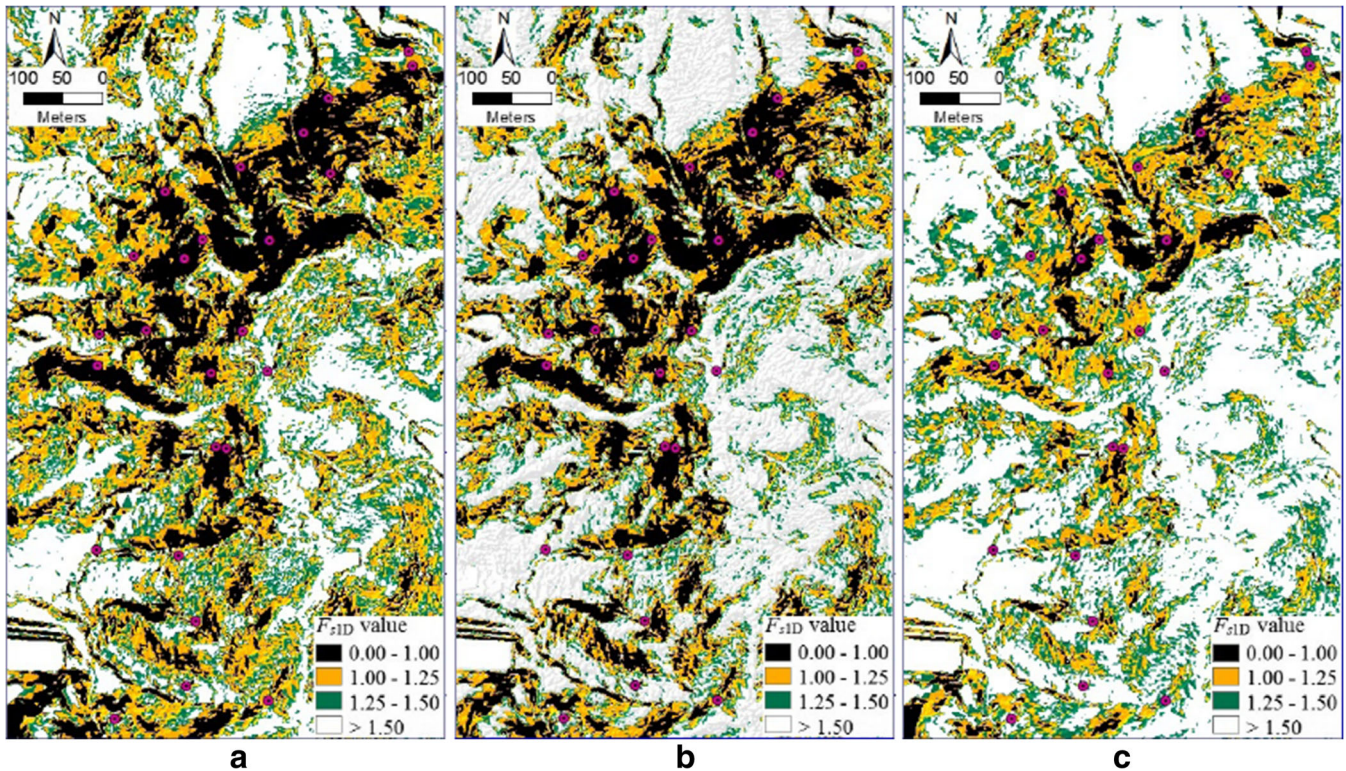| F_s class	LR$_{class}$ (e) = (c)/(d)			%LR$_{class}$ (e)/(f)		
	U	S1	S2	U	S1	S2
$F_s < 1$	2.434	2.98	3.31	79.95	85.64	80.18
$F_s \geq 1$	0.610	0.50	0.82	20.05	14.36	19.82
Sum	3.044 (f)	3.48 (f)	4.13 (f)	100.0	100.0	100.0

Fig. 9 F_{s1D} maps simulated at 09:00 on July 27, 2011, using **a** the U model, **b** S1 model, and **c** S2 model for the soil depth, described in the "Spatial distribution of soil depth" section. The maps are classified in four F_{s1D} intervals for illustration purposes, while the performance assessment is based only on the $F_{s1D} < 1$ and $F_{s1D} \geq 1$ classes, as discussed at the end of the "A performance index for point-like landslide data" section

class of F_s." This is not accurate since not all the area is a slope failure. Therefore, we revised it to "% of predicted areas in each F_s class" as presented in Eq. (6). Moreover, while some authors distinguish the factor-of-safety values in many classes (e.g., Mandal and Maiti (2015)), we consider only the two classes following directly from the very meaning of F_s: stable cells ($F_s \geq 1.0$) and unstable cells ($F_s < 1$). Our choice is motivated by the fact that both definitions of the factor of safety, Eq. (1) for 1D modeling and Eq. (4) for 3D modeling, describe a quantity built as the ratio of destabilizing and resisting forces. As such, there is no room for interpreting F_s in more than two classes, since the balance of forces can only result in either stability or instability. We acknowledge that numerical values of the indexes defined by Eqs. (6) and (7) depend on the number of classes used in the analysis. Nevertheless, we believe that the indexes of Eqs. (6) and (7) provide a reasonable tool for comparing the 1D and 3D models, so long as the comparison is performed in a consistent manner. The application of Eq. (6) and Eq. (7) in validating the predicted landslide results is also explained in Tables 2 and 3.

Results and discussion

The approach adopted in this work aims at assessing the performance of the combined application of the TRIGRS and Scoops3D slope stability models, amounting to an overall spatially distributed and time-dependent prediction of landslide occurrence. We investigated independently the timing and locations of model predictions against data consisting of rainfall measurements of a

particular event known to have triggered landslides, whose locations were known as points. For this reason, we used a synthetic index to compare the pixel-based model output and points approximately representing individual landslides. We could not further investigate the spatial extent of model predictions.

A choice of a specific soil depth map was mandatory to perform meaningful physically based modeling. We choose a specific soil depth map by analyzing the predicted F_s maps obtained using three different soil depth models, as described in the "Spatial distribution of soil depth" section, within TRIGRS and without additional 3D modeling (Fig. 9). A comparison with the observed landslide locations was performed using the %LR$_{class}$ index (Park et al. 2013), as discussed in the "A performance index for point-like landslide data" section. We used this index to analyze stability maps corresponding to the three different soil depth models. Tables 2 and 3 present results for %LR$_{class}$ using the three soil depth models. The final results for %LR$_{class}$ are presented in Table 3, while Table 2 shows intermediate results useful to understand how the synthetic index was calculated. Results in Fig. 9 and Tables 2 and 3 show that soil depth model S1 provided the best performance of TRIGRS in landslide prediction, since it accurately predicted the highest percent of all the sliding sites (60%) with the largest chance of including those landslides (85.64%). Therefore, we use the S1 model hereafter, suggesting in our case a linear relationship between the slope angle and the soil depth.

We analyzed the results obtained from the 1D (TRIGRS only) and 3D (TRIGRS plus Scoops3D) models at 09:00 on July 27, i.e.,
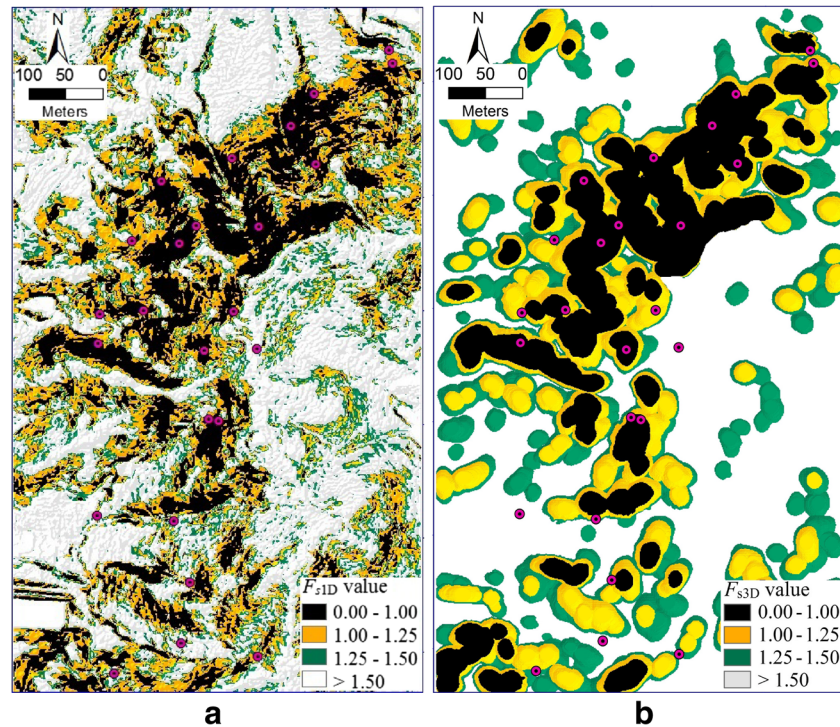
Fig. 10 Factor-of-safety maps calculated at 09:00 on July 27, 2011, within the TRIGRS approach, F_{s1D} (**a**), and the coupled TRIGRS-Scoops3D approach, F_{s3D} (**b**). The maps are classified in four F_s intervals for illustration purposes, while the performance assessment is based only on the $F_s < 1$ and $F_s \geq 1$ classes, as discussed at the end of the "A performance index for point-like landslide data" section. The %LR$_{class}$ values summarizing the results shown in the figure are listed in Table 4

the time when most landslides and debris flows occurred. This allowed us to assess the ability of the two approaches in predicting the landslide locations caused by the observed rainstorm. The resulting map of the former is illustrated in Fig. 10a, and the map corresponding to the latter is in Fig. 10b. The figures show that the 3D approach gives a visually more reasonable result than the 1D method, in terms of slip surface. This is expected since it reflects the fact that all soil columns in the slip surface slide at once. In the 1D method, each pixel (soil column) in the F_{s1D} map has its own F_{s1D} value and is independent of other cells. In addition, in the case of the F_{s3D} map, slip surfaces tend to occur in individual blocks, which makes them readily observable. This differs from the 1D approach, where only the unstable areas are seen, but not the slip surfaces, and assumptions have to be made to cluster unstable pixels together and to define landslide bodies (Alvioli et al. 2016). Lastly, the 1D approach presents scattered unstable cells even in places far from sliding sites, which is not the case for the 3D results.

To gain more insight regarding the comparison between stability maps simulated by 1D and 3D methods, we analyzed the %LR$_{class}$ index corresponding to the results at 09:00 for both cases, as presented in Table 4. We see that even when ignoring the influence of negative pore water pressure, the 3D approach seems to lessen the over-prediction of TRIGRS as anticipated in the "Introduction" section. Note that in both approaches, the same number of observed sites was accurately predicted (15 sites). The unstable areas predicted were 17.72% by the 3D method and 20.10% by the 1D method. Consequently, the %LR$_{class}$ is higher in the 3D case compared to the 1D method, reaching 87.44 versus 85.64%, respectively. These results are acceptable for both approaches given that accurate input data for modeling the initial conditions is not fully available.

Regarding the timing evaluation of the predicted F_s maps, we evaluated two issues: (1) the time dependence of the percent of the unstable area as predicted by the two approaches during

Table 4 Comparison of LR$_{class}$ (Eq. (6)) and %LR$_{class}$ (Eq. (7)) obtained within the 3D (Scoops3D) and 1D (TRIGRS) approaches, both calculated at 09:00 for spatial assessment (see the "Results and discussion" section). The F_{s1D} and F_{s3D} maps that correspond to the results listed in this table are shown in Fig. 10

F_s class	Observed sites (a)		Observed sites (%) (c) = (a)/25 × 100		Predicted area (%) (d)		LR$_{class}$ (e) = (c)/(d)		%LR$_{class}$ (e)/(f)	
	3D	1D	3D	1D	3D	1D	3D	1D	3D	1D
$F_s < 1$	15	15	60.0	60.0	17.72	20.10	3.38	2.98	87.44	85.64
$F_s \geq 1$	10	10	40.0	40.0	82.28	79.90	0.49	0.50	12.56	14.36
Sum	25	25	100	100	100	100	3.87 (f)	3.48 (f)	100.0	100.0

Table 5 Stability classes of the observed and predicted landslides at 06:00 calculated within the 3D (Scoops3D) and 1D (TRIGRS) approaches, both calculated at 06:00 for timing assessment (see the "Results and discussion" section). The $F_S < 1$ class provides a percentage of predicted unstable area that is substantially smaller than the corresponding results at a later time, 09:00, listed in Table 4. The F_{s1D} and F_{s3D} maps that correspond to the results listed in this table are shown in Fig. 12

F_s class	Observed sites		Observed sites (%)		Predicted area (%)	
	3D	1D	3D	1D	3D	1D
$F_s < 1$	5	6	20.0	24.0	6.04	10.2
$F_s \geq 1$	20	19	80.0	76.0	93.96	89.8
Sum	25	25	100.0	100.0	100.0	100.0

the rainfall and (2) the F_s map predicted at the time step right before the critical period when most of the landslides were observed. Figure 11 shows the time dependence of the percent of unstable area predicted by the 1D and 3D approaches during the rainfall event. Both models produced results consistent with the observations since the unstable area is smaller at the beginning of the storm and it increases significantly to the maximum during the critical period (07:00 to 09:00 on July 27 as discussed in the "3D slope stability with the Scoops3D model" section) and stays almost constant after that. The 3D model provides unconditionally unstable areas (a few cells with $F_s < 1$ at $t = 0$, when no rainfall was presented), which can be explained by the assumptions about no negative pore pressure in the 3D model or the assumptions of the soil depth model or the initial groundwater table. The main conclusion, however, is that the timing of both the 1D and 3D models is correct, in that most of the landslides are predicted to occur at the appropriate time.

Thus, to assess quantitatively the timing of the predictions, we analyzed the predicted F_s maps at 06:00 on July 27, the time step right before the critical period of the rainstorm. The number of sliding sites falling within the unstable area in the 06:00 stability map was predicted to occur earlier than expected. The extent of the mismatch provides a measure of the inaccuracy in timing prediction. Figure 12a, b shows the stability maps simulated at 06:00 on July 27 by the two approaches, while Table 5 lists the stability classes extracted from the two figures. We conclude that before the critical

period, the unstable area predicted by Scoops3D is slightly lower than that of TRIGRS (6.04 compared to 10.2%). The observed sliding sites detected by the former are also lower than those of the latter (five sites, as compared to six sites). This means that Scoops3D results help to overcome the over-prediction problems of landslide prediction that are known in 1D landslide models.

In an effort to integrate GIS and 3D column-based slope stability analysis, a few models exist in the literature such as 3DSlopeGIS (Xie and Esaki 2004; Xie et al. 2006a; Xie et al. 2006b) and r.slope.stability (Mergili et al. 2012; Mergili et al. 2014) in GRASS GIS (Neteler and Mitasova 2007). Time dependence is not taken into account in existing 3D models, so their results are typically interpreted as landslide susceptibility (Mergili et al., 2012). We have shown that the time dependence implemented by the software combination used for the present work, by means of pressure head variations in response to time-varying rainfall infiltration at different depths calculated by TRIGRS, is consistent with observations and provides better performance than the 1D approach alone.

Lastly, we stress that the use of 3D approaches to find the slip surface is usually time-consuming. It is worth noting that the issue of long computing time is addressed in the r.slope.stability model, which can be run in parallel on multi-core machines. Scoops3D does not run in a GIS environment nor can it be run in parallel, but the latest TRIGRS v2.1 has built-in parallel processing capabilities, allowing the simulation of very large areas in a short time.
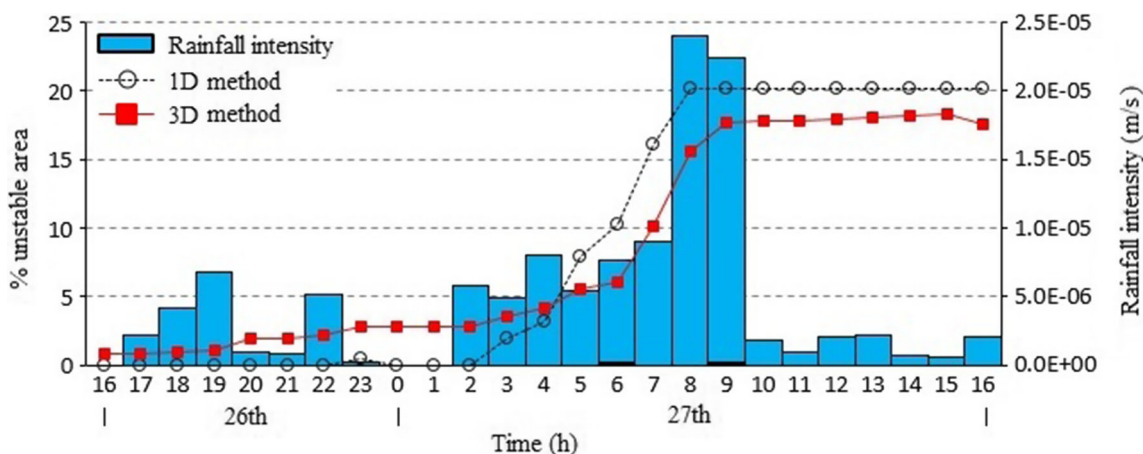

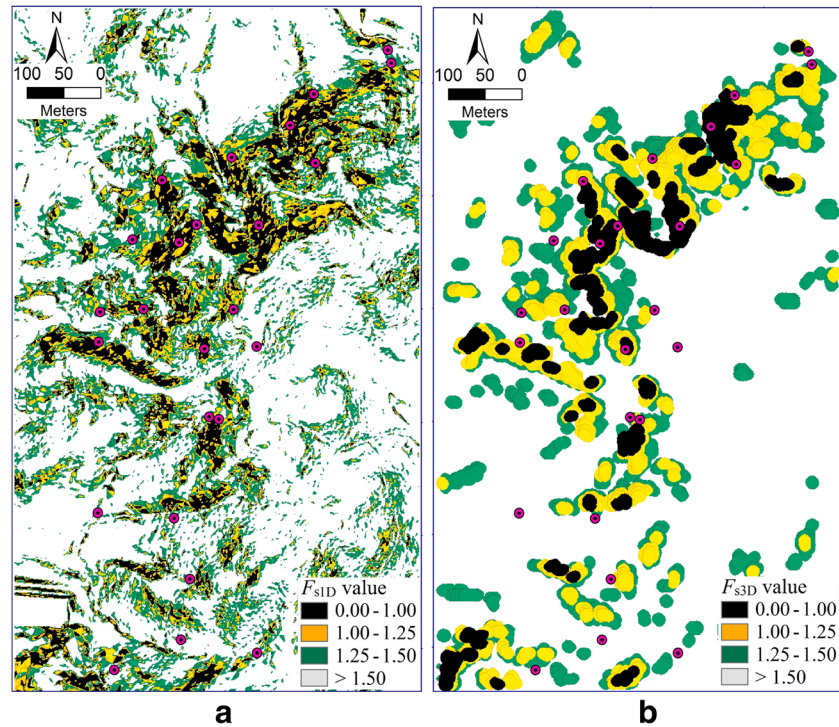**Fig. 11** Time dependence of the percent of unstable area predicted by the 1D and 3D approaches during rainfall

Fig. 12 Factor-of-safety maps calculated at 06:00 on July 27, 2011, within the TRIGRS approach, F_{s1D} (**a**), and the coupled TRIGRS-Scoops3D approach, F_{s3D} (**b**). Note that **a** is identical to Fig. 9. The maps are classified in four F_s intervals for illustration purposes, while the performance assessment is based only on the $F_s < 1$ and $F_s \geq 1$ classes, as discussed at the end of the "A performance index for point-like landslide data" section. The %LR$_{class}$ values summarizing the results shown in the figure are listed in Table 5

Conclusions

In this study, we applied a 3D, time-dependent slope stability method, using the well-known TRIGRS model combined with Scoops3D, thanks to the possibility of integrating the two softwares included in the latest TRIGRS, v2.1. We used the TRIGRS infiltration model to simulate the time-varying hydraulic conditions induced by a rainstorm. We ran Scoops3D using the calculated hydraulic conditions, with the modeling chain amounting to an overall spatially distributed and time-dependent 3D slope stability assessment. We used the information available regarding the landslide event of Mount Umyeon in July 2011 for comparison. We make use of a slightly modified performance index specifically introduced in the literature for comparing pixel-based predictions with point locations for observed landslide initiation, such as the data available for this study. We compared F_s maps predicted by the 1D (TRIGRS) and 3D (TRIGRS plus Scoops3D) approaches with existing landslide data, within the limitations imposed by the different kinds of landslides described by the two models.

The TRIGRS and Scoops3D models have different purposes and scopes, with the former intended to predict shallow landslides, while the latter was developed to describe rotational landslides, although a truncation of the ellipsoidal shape can be requested to mimic shallow landslide mechanisms. Our comparison is understood to be valid within the limitations dictated by the mentioned differences. These limitations can be reconciled considering that in landslide data, only the initiation locations of landslides were known to us, and no attempt was made to describe the downslope movement of the mobilized material after the rainfall-triggered

slope failures. We found that the 3D method is clearly more realistic than the 1D method with respect to slip surface definition, as expected. From the results obtained within this approach, presented in the "Results and discussion" section, several conclusions can be drawn:

1. TRIGRS allows the choice of a specific soil depth model. Among three approaches, a soil thickness linearly proportional to the slope angle showed the best performance of TRIGRS in landslide prediction within the %LR$_{class}$ index assessment.
2. Concerning landslide location assessment, although some input data was not available (including soil depth and soil diffusivity, among others), F_{s3D} maps predicted almost 87.44% of the observed landslides (that is, if a landslide occurs, the predicted unstable area ($F_s < 1$) has an 87.44% chance of including the actual landslides). Out of the 25 observed sliding sites, 60% were accurately detected.
3. Concerning landslide timing assessment, Scoops3D combined with TRIGRS proved to be a valuable tool in our case study. The results indicate that most of the predicted landslides tend to occur in the correct period of time (from 07:00 to 09:00 KST on July 27). Before the critical period (07:00 to 09:00), only 6.04% of the whole area was predicted as unstable. However, the unstable area increased to 17.72% at 09:00. Almost 67% the observed sliding sites are predicted to occur at the right time, as the other 33% took place before 06:00.
4. It is shown that Scoops3D has the potential to overcome the over-prediction problems of landslide prediction in terms of

both location and timing of the occurrence, known to be present in 1D landslide models. A moderate improvement in the %LR$_{class}$ index is also observed in the 3D method as compared to the 1D method (87.44 versus 85.64%). We suggest the %LR$_{classs}$, introduced by Park et al. (2013) for pixel-based versus point-like modeling, be used with the only two $F_s < 1$ and $F_s \geq 1$ classes in agreement with the F_s definition and meaning.

In conclusion, it is convinced that this combined TRIGRS-Scoops3D approach is an effective tool for 3D, spatially distributed and time-dependent assessment of rainfall-induced landslides. Further developments of this work include expert mapping of the orthophotographs, as in, e.g., Guzzetti et al. (2012), of the study area to determine the actual size and shape of each landslide. Such improvement will help provide a detailed evaluation of the sizes of landslide-triggering areas, thus allowing a cell-by-cell comparison between model predictions and field reality. Furthermore, future research in the Mount Umyeon study area should also provide modeling and validation of the downslope movement of the mobilized material with advanced tools, such as the ones proposed by Chianga et al. (2012), Gomes et al. (2013), or the recently proposed open-source model r.awaflow (Mergili et al. 2012), also operated in a GIS framework.

Acknowledgments

References

Alvioli M, Baum RL (2016) Parallelization of the TRIGRS model for rainfall-induced landslides using the message passing interface. Environ Model Soft 81:122–135. https://doi.org/10.1016/j.envsoft.2016.04.002

Alvioli M, Guzzetti F, Rossi M (2016) Scaling properties of rainfall-induced landslides predicted by a physically based model. Geomorphology 213:38–47. https://doi.org/10.1016/j.geomorph.2013.12.039

An H, Viet TT, Lee GH, Kim Y, Kim M, Noh S, Noh J (2016) Development of time-variant landslide-prediction software considering three-dimensional subsurface unsaturated flow. Environ Model Soft 85:172–183. https://doi.org/10.1016/j.envsoft.2016.08.009

Arellano D, Stark T (2000) Importance of three-dimensional slope stability analyses in practice. Paper presented at the Geo-Denver 2000. Denver. American Society of Civil Engineers, pp 19-33. doi: https://doi.org/10.1061/40512(289)2

Askarinejad A, Casini F, Bischof P, Beck A, Springman SM (2012) Rainfall induced instabilities: a field experiment on a silty sand slope in northern Switzerland. Italian Geotech J 46(3):50–71

Baek MH, Kim TH (2015) A study on the use of planarity for quick identification of potential landslide hazard. Nat Hazards Earth Syst Sci. 15:997–1009. https://doi.org/10.5194/nhess-15-997-2015

Baum RL, Godt JW, Savage WZ (2010) Estimating the timing and location of shallow rainfall-induced landslides using a model for transient, unsaturated infiltration. J Geophys Res 115:F03013. https://doi.org/10.1029/2009JF001321

Baum RL, Savage WZ, Godt JW (2008) TRIGRS - A fortran program for transient rainfall infiltration and grid - based regional slope-stability analysis, Version 2.0. USGS Open File Report 08-1159

Bishop AW (1955) The use of the Slip Circle in the Stability Analysis of Slopes. Geotechnique 5(1):7–17. https://doi.org/10.1680/geot.1955.5.1.7

Brien DL, Reid ME (2007) Modeling 3-D slope stability of coastal bluffs, using 3-D ground-water flow, Southwestern Seattle, Washington. Retrieved from U.S. Geological Survey, pp 1-54

Bromhead EN, Ibsen ML, Papanastassiou X, Zemichael AA (2002) Three-dimensional stability analysis of a coastal landslide at Hanover Point, Isle of Wight. Quart J Eng Geol Hydrogeol 35(1):79–88. https://doi.org/10.1144/qjegh.35.1.79

Catani F, Segoni S, Falorni G (2010) An empirical geomorphology-based approach to the spatial prediction of soil thickness at catchment scale. Water Resources Research 46(5):1–15. https://doi.org/10.1029/2008WR007450 2010

Chakraborty A, Goswami D (2016) State of the art: Three dimensional (3D) slope-stability analysis. International Journal of Geotechnical Engineering 10(5):1–6. https://doi.org/10.1080/19386362.2016.1172807

Chiang SH, Chang KT, Mondini AC, Tsai BW, Chen CY (2012) Simulation of event-based landslides and debris flows at watershed level. Geomorphology 138 (1):306–318. https://doi.org/10.1016/j.geomorph.2011.09.016

Gens A, Hutchinson JN, Cavounidis S (1988) Three-dimensional analysis of slides in cohesive soils. Geotechnique 38(1):1–23. https://doi.org/10.1680/geot.1988.38.1.1

Gomes RAT, Guimarães RF, Carvalho OA, Fernandes NF, Amaral Júnior EV (2013) Combining Spatial Models for Shallow Landslides and Debris-Flows Prediction. Remote Sens 5(5):2219–2237. https://doi.org/10.3390/rs5052219

Gu T, Wang J, Fu X, Liu Y (2014) GIS and limit equilibrium in the assessment of regional slope stability and mapping of landslide susceptibility. Bull Eng Geol Environ 74(4):1105–1115. https://doi.org/10.1007/s10064-014-0689-2

Guzzetti F, Mondini AC, Cardinali M, Fiorucci F, Santangelo M, Chang KT (2012) Landslide inventory maps: New tools for an old problem. Earth Sci Rev 112(1-2):42–66. https://doi.org/10.1016/j.earscirev.2012.02.001

Hovland HJ (1977) Three-dimensional slope stability analysis method. J Geotech Eng Div ASCE 103(9):971–986

Huang CC, Tsai CC (2000) New method for 3D and asymmetrical slope stability analysis. J Geotechnical Geoenviron Eng 126(10):917–927. https://doi.org/10.1061/(ASCE)1090-0241(2000)126:10(917)

Hungr O (1987) An extension of Bishop's simplified method of slope stability analysis to three dimensions. Geotechnique 37(1):113–117. https://doi.org/10.1680/geot.1987.37.1.113

Hungr O (1995) A model for the runout analysis of rapid flow slides, debris flows, and avalanches. canadienne de géotechnique 32(4):610–623. https://doi.org/10.1139/t95-063

Hungr O, Salgado FM, Byrne PM (1989) Evaluation of three-dimensional method of slope stability analysis. Can Geotech J 26:679–686. https://doi.org/10.1139/t89-079

Hürlimann M, Rickenmann D, Medina V, Bateman A (2008) Evaluation of approaches to calculate debris-flow parameters for hazard assessment. Eng Geol 102(3-4):152–163. https://doi.org/10.1016/j.enggeo.2008.03.012

Iverson RM (1997) The Physics of debris flows. Reviews of Geophysics 35(3):245–296. https://doi.org/10.1029/97RG00426

Jeong S, Kim Y, Lee JK (2015) The 27 July 2011 debris flows at Umyeonsan, Seoul, Korea. Landslides 12:799–813. https://doi.org/10.1007/s10346-015-0595-0

Jia N, Yang Z, Xie M, Mitani Y, Tong J (2014) GIS-based three-dimensional slope stability analysis considering rainfall infiltration. Eng Geol Environ. 74(3):919–931. https://doi.org/10.1007/s10064-014-0661-1

Kalatehjari R, Ali N (2013) A Review of three-dimensional slope stability analyses based on limit equilibrium method. Electronic Journal of Geotechnical Engineering 18:119–134

Kim D, Im S, Lee SH, Hong Y, Cha KS (2010) Predicting the rainfall-triggered landslides in a forested mountain region using TRIGRS model. J Mt Sci 7(1):83–91. https://doi.org/10.1007/s11629-010-1072-9

Kim D, Lee EJ, Ahn B, Im S (2014) Landslide Susceptibility Mapping Using a Grid-based Infiltration Transient Model in Mountainous Regions. In: Sassa K, Canuti P, Yin Y (eds) Landslide Science for a Safer Geoenvironment, Methods of Landslide Studies, vol 2. Springer International Publishing. doi, Cham, pp 425–429. https://doi.org/10.1007/978-3-319-05050-8_66

Korean Society of Civil Engineers (2011) Research contract report: causes survey and restoration work of Mt. Woomyeon landslide 2012

Lam L, Fredlund DG (1993) A general limit-equilibrium model for three-dimensional slope stability analysis. Can Geotech J 30:905–919. https://doi.org/10.1139/t93-089

Mandal S, Maiti R (2015) Semi-quantitative approaches for landslide assessment and prediction. New York: Springer Natural Hazards. https://doi.org/10.1007/978-981-287-146-6

Mergili M, Marchesini I, Rossi M, Guzzetti F, Fellin W (2012) Spatially distributed three-dimensional slope stability modelling in a raster GIS. Geomorphology 206:178–195. https://doi.org/10.1016/j.geomorph.2013.10.008

Mergili M, Marchesini I, Alvioli M, Metz M, Schneider-Muntau B, Rossi M, Guzzetti F (2014) A strategy for GIS-based 3-D slope stability modelling over large areas. Geosci Model Dev. 7:2969–2982. https://doi.org/10.5194/gmd-7-2969-2014

Miller DJ, Sias J (1998) Deciphering large landslides: linking hydrological, groundwater and slope stability models through GIS. Hydrological Processes 12(6):923–941. https://doi.org/10.1002/(SICI)1099-1085(199805)12:6<923::AID-HYP663>3.0.CO;2-3

Montgomery DR, Dietrich WE (1994) A physically based model for the topographic control on shallow landsliding. Water Resources Research 30(4):1153–1171. https://doi.org/10.1029/93WR02979

Neteler M, Mitasova H (2007) Open Source GIS: A GRASS GIS Approach. Springer, New York

Okimura T (1994) Prediction of the shape of a shallow failure on a mountain slope: The three-dimensional multi-planar sliding surface method. Geomorphology 9:223–233. https://doi.org/10.1016/0169-555X(94)90064-7

Pack RT, Tarboton DG, Goodwin CN (1998) SINMAP 2.0 - A stability index approach to terrain stability hazard mapping, user's manual. Utah state university: Canadian Forest Products Ltd.

Park DW, Nikhil NV, Lee SR (2013) Landslide and debris flow susceptibility zonation using TRIGRS for the 2011 Seoul landslide event. Nat Hazards Earth Syst Sci 13:2833–2849. https://doi.org/10.5194/nhess-13-2833-2013

Pelletier JD, Rasmussen C (2009) Geomorphically based predictive mapping of soil thickness in upland watersheds. Waster Resour Res 45(9):1–15. https://doi.org/10.1029/2008WR007319

Quiu C, Xie M, Esaki T (2007) Application of GIS Technique in Three-Dimensional Slope Stability Analysis. Paper presented at the International Symposium on Computational Mechanics, Beijing, China. Computational Mechanics:316–316. https://doi.org/10.1007/978-3-540-75999-7_116

Raia S, Alvioli M, Rossi M, Baum RL, Godt JW, Guzzetti F (2014) Improving predictive power of physically based rainfall-induced shallow landslide models: a probabilistic approach. Geosci Model Dev 7:495–514. https://doi.org/10.5194/gmd-7-495-2014

Reid ME, Christian SB, Brien DL (2000) Gravitational stability of three-dimensional stratovolcano edifices. Journal of Geophysical Research 105(B3):6043–6056. https://doi.org/10.1029/1999JB900310

Reid ME, Christian SB, Brien DL, Henderson ST (2015) Scoops3D—software to analyze three-dimensional slope stability throughout a digital landscape (Version 1.0). Virginia: U.S. Geological Survey

Reid ME, Keith EC, Kayen RE, Iverson NR, Iverson RM, Brien DL (2010) Volcano collapse promoted by progressive strength reduction: new data from Mount St. Helens. Bull Volcanol 72:761–766. https://doi.org/10.1007/s00445-010-0377-4

Salciarini D, Godt J, Savage WZ, Conversini P, Baum RL, Michael JA (2006) Modeling regional initiation of rainfall-induced shallow landslides in the eastern Umbria Region of central Italy. Landslides 3(3):181–194. https://doi.org/10.1007/s10346-006-0037-0

Saulniera GM, Bevenb K, Obleda C (1997) Including spatially variable effective soil depths in TOPMODEL. Journal of Hydrology 202(1-4):158–172. https://doi.org/10.1016/S0022-1694(97)00059-0

Spencer E (1967) A method of analysis the stability of embankments assuming parallel inter-slice forces. Geotechnique 17(1):11–26. https://doi.org/10.1680/geot.1967.17.1.11

Taylor DW (1948) Fundamentals of soil mechanics. John Wiley & sons, Inc., New York

Tesfa TK, Tarboton DG, Chandler DG, McNamara JP (2009) Modeling soil depth from topographic and land cover attributes. Water Resources Research 45(10):1–16. https://doi.org/10.1029/2008WR007474

Tran TV, Lee GH, An H, Kim M (2017) Comparing the performance of TRIGRS and TiVaSS in spatial and temporal prediction of rainfall-induced shallow landslides. Environ Earth Sci 76(315):1–16. https://doi.org/10.1007/s12665-017-6635-4

Trigila A, Iadanza C, Spizzichino D (2010) Quality assessment of the Italian Landslide Inventory using GIS processing. Landslides 7(4):455–470. https://doi.org/10.1007/s10346-010-0213-0

Valentino R, Meisina C, Montrasio L, Losi GL, Zizioli D (2014) Predictive power evaluation of a physically based model for shallow landslides in the area of Oltrepo` Pavese, Northern Italy. Geotech Geol Eng 32(4):783–805. https://doi.org/10.1007/s10706-014-9758-3

Vallance JW, Schilling SP, Devoli G, Reid ME, Howell MM, Brien DL (1998) Lahar Hazards at Casita and San Cristóbal Volcanoes, Nicaragua. Retrieved from Vancouver, Washington U.S.A. U.S. Geological Survey. pp 1-24

Viet TT, Lee G, Thu TM, An HU (2016) Effect of DEM resolution on shallow landslide modeling using TRIGRS. Nat Hazards Rev 18(2):1–12. https://doi.org/10.1061/(ASCE)NH.1527-6996.0000233.

Xie M, Esaki T (2004) GIS-based probabilistic mapping of landslide hazard using a three-dimensional deterministic Model. Natural Hazards 33:265–282. https://doi.org/10.1023/B:NHAZ.0000037036.01850.0d

Xie M, Esaki T, Cai M (2006a) GIS-Based Implementation of Three-Dimensional Limit Equilibrium Approach of Slope Stability. J Geotech Geoenviron Eng 132:656–660. https://doi.org/10.1061/ASCE1090-02412006132:5656

Xie M, Esaki T, Qiu C, Wang C (2006b) Geographical information system-based computational implementation and application of spatial three-dimensional slope stability analysis. Computers and Geotechnics 33:260–274. https://doi.org/10.1016/j.compgeo.2006.07.003

Yu HS, Salgado R, Sloan SW, Kim JM (1998) Limit analysis versus limit equilibrium for slope stability. J Geotech Geoenviron Eng 124(1):1–11. https://doi.org/10.1061/(ASCE)1090-0241(1998)124:1(1)

T. V. Tran (✉)
Department of Civil Engineering,
Thuyloi University,
Hanoi, Vietnam
Email: trantheviet@tlu.edu.vn

T. V. Tran · G. Lee
Department of Construction & Disaster Prevention Engineering,
Kyungpook National University,
Sangju, South Korea

M. Alvioli
Consiglio Nazionale delle Ricerche,
Istituto di Ricerca per la Protezione Idrogeologica,
Via Madonna Alta 126, 06128, Perugia, Italy

H. U. An
Department of Agricultural and Rural Engineering,
Chungnam National University,
Daejeon, South Korea